Human Molecular Genetics, 2020, Vol. 29, No. 11 1772–1783

doi: 10.1093/hmg/ddz108
Advance Access Publication Date: 21 May 2019
General Article

GENERAL ARTICLE

Activating *MRAS* mutations cause Noonan syndrome associated with hypertrophic cardiomyopathy

Marialetizia Motta[1,†], Lena Sagi-Dain[2,†], Oliver H.F. Krumbach[3], Andreas Hahn[4], Amir Peleg[2], Alina German[5], Christina Lissewski[6], Simona Coppola[7], Francesca Pantaleoni[1], Luisa Kocherscheid[6], Franziska Altmüller[6], Denny Schanze[6], Thushiha Logeswaran[8], Soheyla Chahrokh-Zadeh[9], Anna Munzig[9], Saeideh Nakhaei-Rad[3,‡], Hélène Cavé[10,11], Mohammad R. Ahmadian[3], Marco Tartaglia[1,§,*] and Martin Zenker[6,§]

[1]Genetics and Rare Diseases Research Division, Ospedale Pediatrico Bambino Gesù, IRCCS, Rome, Italy, [2]The Human Genetic institute, Carmel Medical Center, Ruth and Bruce Rappaport Faculty of Medicine, Israel Institute of Technology, Haifa, Israel, [3]Institute of Biochemistry and Molecular Biology II, Medical Faculty of the Heinrich Heine University, Düsseldorf, Germany, [4]Department of Child Neurology, University Hospital, Gießen, Germany, [5]Pediatric Department, Bnai-Zion Medical Center and Clalit Health Maintenance Organization, Haifa, Israel, [6]Institute of Human Genetics, University Hospital, Magdeburg, Germany, [7]National Centre for Rare Diseases, Istituto Superiore di Sanità, Rome, Italy, [8]Pediatric Heart Center, University Hospital, Gießen, Germany, [9]Center of Human Genetics and Laboratory Diagnostics, Martinsried, Germany, [10]Assistance Publique des Hôpitaux de Paris (AP-HP), Hôpital Robert Debré, Département de Génétique, 75019 Paris, France and [11]INSERM UMR 1131, Institut de Recherche Saint-Louis, Université de Paris, 75010 Paris, France

[*]**To whom correspondence should be addressed at** Genetics and Rare Diseases Research Division, Ospedale Pediatrico Bambino Gesù, Viale di San Paolo 15, 00146 Rome, Italy. Phone: +39 06 68593742; Fax: +39 06 68594584; Email: marco.tartaglia@opbg.net

Abstract

The RASopathies are a group of genetic syndromes caused by upregulated RAS signaling. Noonan syndrome (NS), the most common entity among the RASopathies, is characterized mainly by short stature, cardiac anomalies and distinctive facial features. Mutations in multiple RAS-MAPK pathway-related genes have been associated with NS and related phenotypes. We describe two unrelated patients presenting with hypertrophic cardiomyopathy (HCM) and dysmorphic features suggestive of NS. One of them died in the neonatal period because of cardiac failure. Targeted sequencing revealed *de novo* *MRAS* variants, c.203C > T (p.Thr68Ile) and c.67G > C (p.Gly23Arg) as causative events. *MRAS* has only recently been related to NS based on the observation of two unrelated affected individuals with *de novo* variants involving the same codons here

[†]These authors contributed equally to this work.
[‡]Current address: Stem Cell Biology and Regenerative Medicine, Institute of Biotechnology, Ferdowsi University of Mashhad, Mashhad, Iran.
[§] ^These authors jointly coordinated this work.

Received: April 11, 2019. **Revised:** May 14, 2019. **Accepted:** May 14, 2019

found mutated. Gly23 and Thr68 are highly conserved residues, and the corresponding codons are known hotspots for RASopathy-associated mutations in other RAS proteins. Functional analyses documented high level of activation of MRAS mutants due to impaired GTPase activity, which was associated with constitutive plasma membrane targeting, prolonged localization in non-raft microdomains, enhanced binding to PPP1CB and SHOC2 protein, and variably increased MAPK and PI3K-AKT activation. This report provides additional evidence that a narrow spectrum of activating mutations in *MRAS* represents another rare cause of NS, and that *MRAS* has to be counted among the RASopathy genes predisposing to HCM. Moreover, our findings further emphasize the relevance of the MRAS-SHOC2-PPP1CB axis in the control of MAPK signaling, and the contribution of both MAPK and PI3K-AKT pathways in MRAS functional upregulation.

Introduction

The RASopathies are a group of genetic disorders caused by germline mutations in genes that encode components and regulators of the RAS/mitogen activated protein kinase (MAPK) pathway, an intracellular signaling cascade that is involved in many cellular, developmental and physiological processes (1–3). Taken together, the RASopathies represent the most common non-chromosomal diseases affecting development, with an estimated prevalence of 1 in 2000 individuals. This clinically variable group of disorders includes Noonan syndrome (NS, OMIM PS163950), Costello syndrome (OMIM 218040), cardiofaciocutaneous syndrome (OMIM PS115150), NS with multiple lentigines (LEOPARD syndrome; OMIM PS151100), Mazzanti syndrome (NS-like disorder with loose anagen hair; OMIM PS607721), neurofibromatosis type 1 (OMIM 162200), Legius syndrome (OMIM 611431), and an increasing number of related conditions. These disorders share some major clinical features, such as a distinctive pattern of facial dysmorphisms, post-natal growth failure, cutaneous, cardiac and skeletal defects, cognitive deficits, behavioral abnormalities, and a variable increased risk for cancer (1–3).

NS, the most common entity among the RASopathies, is characterized mainly by short stature, a wide spectrum of congenital cardiac anomalies and hypertrophic cardiomyopathy (HCM) (50%–80% of the affected subjects), and a recognizable facies, which includes hypertelorism with down-slanting palpebral fissures and low-set, posteriorly rotated ears as major features (4,5). In addition, patients with NS show an increased risk for bleeding disorders and certain malignancies, and may have variable developmental delay and cognitive deficits. The syndrome has been associated with mutations in more than 10 genes (6), and it is mainly transmitted as an autosomal dominant trait with a high proportion of *de novo* mutations, although a recessive form of NS related to biallelic inactivating/hypomorphic mutations in *LZTR1* gene (OMIM #600574) has recently been recognized and characterized (7–9). Mutations affect genes encoding signal transducers participating in the RAS-MAPK backbone as well as proteins functioning in signaling circuits with positive or negative modulatory role on this signaling cascade. While this evidence strongly points to the upregulation of MAPK signaling as a major event implicated in disease pathogenesis, the contribution of other signaling pathways to disease pathogenesis has recently been suggested and documented (10–14). Notably, several clinically relevant genotype-phenotype correlations have been recognized. Among these, an increased prevalence of HCM among affected subjects heterozygous for a specific class of missense mutations in *RAF1*, and mutations affecting the *RIT1* and *LZTR1* genes has been described (15–20).

One of the genes recently reported to be implicated in NS is *MRAS* (MIM #608435), encoding a small monomeric GTPase belonging to the RAS family controlling multiple signaling pathways, including the MAPK and PI3K-AKT cascades (20,21). One subject with clinical diagnosis of NS showing HCM as associated feature was reported to carry a *de novo* missense mutation (p.Gly23Val) that was documented to stabilize MRAS in its active conformation, and to slightly enhance signaling through the MAPK cascade (22). The same team identified a second subject carrying a different *de novo MRAS* variant (p.Thr68Ile) among a relatively large cohort of mutation-negative patients with clinical diagnosis of NS associated with HCM (22), pointing to *MRAS* as a novel disease gene implicated in NS and predisposing to HCM, when mutated.

In this work, we report on two patients with clinical features of NS caused by a *de novo* activating mutation of *MRAS*, representing the third and fourth individual with this particular genetic etiology reported to date. We characterize the biochemical consequences of the three NS-causing mutations reported thus far on MRAS protein behavior and demonstrate their activating effect in modulating the MAPK and PI3K-AKT cascades, with the former found to be upregulated in a cell-specific manner. We also provide evidence that the upregulation of MAPK signaling is associated with enhanced binding of the three NS-causing MRAS mutants to PPP1CB and SHOC2 proteins, confirming further the relevance of the MRAS-SHOC2-PPP1CB complex in positively modulating MAPK signaling. The presence of cardiac hypertrophy in all reported individuals with *MRAS* mutations suggests that *MRAS* has to be counted among the RASopathy genes predisposing to HCM, further emphasizing the importance of a comprehensive mutation screening approach for a more effective patient management.

Results

Clinical description

Patient 1, first child of healthy non-consanguineous, North African Jewish parents, was born after 38 weeks of an uneventful pregnancy and was delivered without complications. His birth weight, head circumference and body length were 2945 g (−1.1 SD), 33.5 cm (−1.1 SD) and 47 cm (−1.6 SD), respectively. Apgar score was 9/10, and initial physical examination noted only mild pectus excavatum. Three days after the delivery, the patient was admitted to neonatal intensive care unit due to dyspnea and treated by intravenous antibiotics due to suspected pneumonia. Echocardiography at the age of four days demonstrated a patent foramen ovale and an atrial septal defect. After recovery from his infection the patient was discharged at age 10 days. Repeated echocardiography at age 10 months revealed dilatation of coronary sinus, with normal ventricular function. However, at age 14 months mild left ventricular hypertrophy was first noted, together with a small septal

defect causing left-to-right shunting. At the age of 15 months, growth delay with appropriate weight was noted (height and weight at −2.0 SD), along with obstructive sleep apnea. Ophthalmological examination demonstrated intermittent exotropia, mainly on the right. The patient was hospitalized few times due to infectious diseases (RSV bronchiolitis at age four months, and recurrent otitis media and infectious mononucleosis at age 15 months). Sweat test and nasal nitric oxide were normal. Audiological examination showed moderate hearing loss due to middle ear effusions. At age 20 months, adenoidectomy and myringotomy with hollow tube insertion were performed. Independent walking was achieved at the age of 17 months. At age two years, the child had no active speech and was diagnosed with mild global developmental delay. Endocrinological evaluation at that age showed normal levels of prolactin, IGF1, IGFBP3, and thyroid function tests. However, glucagon stimulation test was suggestive of growth hormone (GH) deficiency (GH values ranging from 1.1 to 4.2 µg/L, lower than the accepted cutoff of 7.5 µg/L). The patient was referred for genetic evaluation at age two years and three months. His height and weight were both slightly below normal values (82 cm and 10.7 kg, respectively; both −2.0 SD), head circumference was 47.5 cm (+1.0 SD). Facial features were suggestive of NS, with hypertelorism, downslanting palpebral fissures, palpebral ptosis, a short bulbous nose with low nasal bridge and upturned nostrils, long and smooth philtrum, full drooping cheeks with prominent nasolabial folds, small mouth, and mild retrognathia. Parents declined the publication of photos, but the evaluation of the craniofacial phenotype by a RASopathy expert (M.Z.) confirmed it to be typical of NS. In addition, evaluation of the facial photograph using face2gene (https://www.face2gene.com/) yielded NS and cardiofaciocutaneous syndrome as the best hits. One café-au-lait spot sized 10x3 mm was noted on his right lower abdomen, as well as mild pectus excavatum and relatively thin scalp hair. Following the genetic diagnosis, treatment with GH was started. Follow-up neurodevelopmental evaluation showed significant global developmental delay in all fields (Developmental Quotient score of 56). Echocardiography at the age of 3 years documented concentric hypertrophy of cardiac ventricles.

Patient 2, a first child of healthy, non-consanguineous German parents, was born spontaneously without complications at 37 gestational weeks after uneventful pregnancy. Apgar scores were 6/8/10 and umbilical cord pH was 7.34. Her birth weight was 3440 g (+0.5 SD), length was 49 cm (−0.7 SD), and head circumference was 34 cm (−0.5 SD). Respiratory distress was noticed immediately after birth and required CPAP support. Clinical examination showed a short neck with excess skin folds, low set ears, a broad forehead, mild ptosis, hypertelorism, and a systolic heart murmur. X-ray examination of the chest and echocardiography were performed because of persistent tachydyspnea without laboratory signs of a neonatal infection. These tests disclosed significant cardiomegaly (Fig. 1A) with marked biventricular hypertrophic cardiomyopathy (HCM). The patient was treated with propranolol. Although respiratory support could be discontinued after two weeks, cardiac hypertrophy worsened, obstruction of the left-ventricular outflow tract occurred, and cardiac function declined. At age four weeks, echocardiography revealed HCM with severe diastolic dysfunction and mitral valve insufficiency grade 3. Interventricular septal (IVS) thickness was 12 mm (z-score + 5.6) during diastole and 15 mm (z-score + 6) during systole. Left-ventricular posterior wall thickness was 10 mm (z-score + 5.4) during diastole and 12 mm (z-score + 5.6) during systole. The left ventricular outflow gradient was increased to 70 mmHg reflecting marked obstruction (Fig. 1B, C). In addition, an increasing obstruction of the right ventricular outflow tract with a moderate stenosis of 35 mmHg was observed. A RASopathy was suspected because of the facial gestalt in conjunction with the severe biventricular obstructive HCM. After discussing the limited therapeutic options with the parents, they voted for palliative care. The girl was discharged home and deceased at age two months due to cardiac failure. Facial photos are not available.

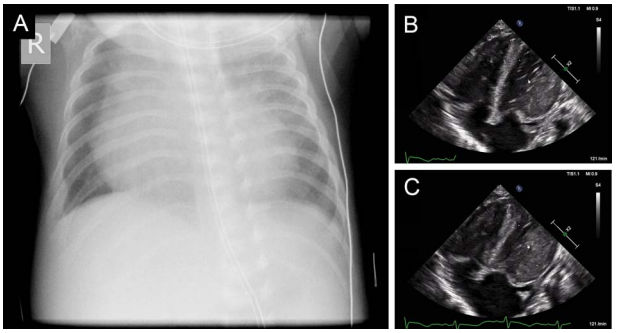

Figure 1. X-ray and echocardiographic findings in patient 2. A, Chest x-ray of the patient at birth revealing marked cardiomegaly. **B**-**C**, Echocardiography during diastole (**B**) and systole (**C**) of the patient at age 4 weeks demonstrating biventricular hypertrophy, increased echogenicity, 'kissing' phenomenon of the left ventricular walls during systole, and substantially reduced left ventricular lumen during systole.

Mutation analyses

In patient 1, multi-gene panel sequencing identified a heterozygous missense variant c.203C > T in exon 3 of *MRAS*, predicting the substitution of a threonine residue by isoleucine (p.Thr68Ile) (Supplementary Material, Fig. S1). No other variants in NS-related genes were qualified as clinically relevant. Molecular genetic testing of both parents excluded the *MRAS* variant in leukocyte DNA, indicating a *de novo* origin of the missense substitution. The identical sequence change in this gene had recently been reported as a *de novo* event in a patient affected by NS with cardiac hypertrophy (22). Patient 1 belonged to a cohort of 288 individuals with a clinical diagnosis of a RASopathy who had previously been tested negative for all known RASopathy-associated genes. The absence of a specific bias in enrollment of these subjects suggest that *MRAS* mutations account for a very small proportion of NS cases. In patient 2, multi-gene panel sequencing revealed the heterozygous *MRAS* missense variant, c.67G > C (p.Gly23Arg), which was again confirmed to be *de novo* (not present in parental leukocyte DNA samples) (Supplementary Material, Fig. S1). A different amino acid substitution at the same codon, p.Gly23Val, had been reported as NS-causing mutation previously (22). Both variants were not reported in major databases (ExAC, gnomAD, 1000G) (Supplementary Material, Table S1). The amino acid residues corresponding to Gly^{23} and Thr^{68} in MRAS are highly conserved in all RAS paralogs and orthologs, from bacteria to mammals (Supplementary Material, Fig. S2). According to various prediction programs, the variants were consistently predicted as pathogenic (Supplementary Material, Table S1). Finally, *MRAS* mutation scan was also performed on a cohort of 1840 consecutive patients with clinical diagnosis of RASopathy or having a phenotype suggestive of these disorders. No putative pathogenic *MRAS* change was identified, while a large proportion of subjects

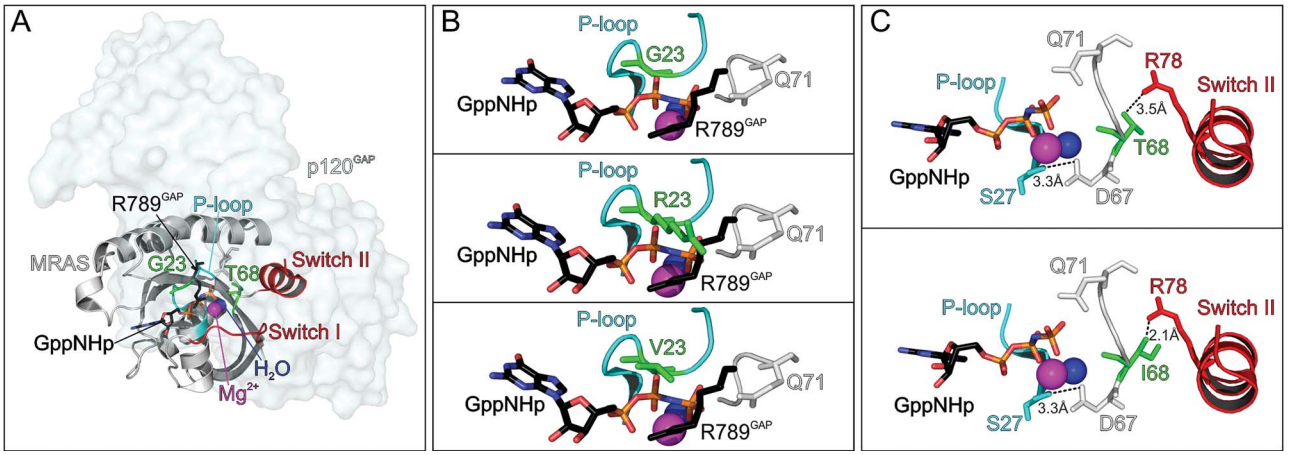

Figure 2. Location of disease-causing *MRAS* mutations and their structural impact. A, Structural modeling of MRAS in complex with p120 RASGAP showing conserved regions and the positions of affected residues. Gly^{23} and Thr^{68}, which are affected in Noonan syndrome, are shown (green), together with the catalytic Arg^{789} of p120 RASGAP. **B**, Gly^{23} (upper panel) is located in the P-loop of MRAS, which is involved in GDP/GTP binding. Arg^{789} of p120 RASGAP interacts with the P-loop and the catalytic Gln^{71}, and stimulates GTP hydrolysis by stabilizing the transition state of this reaction. Substitution of the glycine residue by arginine (middle panel) or valine (lower panel) lead to steric clashes of this interaction, and consequently in an impaired RASGAP function to stimulate the GTPase reaction; as a consequence, MRAS accumulates in its active form. **C**, Thr^{68} is located in the interswitch region of MRAS stabilizing the active site. Asp^{67} of MRAS interacts with Ser^{27} and a water molecule, leading to an indirect interaction with the Mg^{2+} ion and stabilizing the conformation of the switch regions (upper panel). Substitution by isoleucine (lower panel) is predicted to lead to a stronger interaction with Arg^{78} of the switch II region, and potentiate the interaction with effector proteins.

was found positive for disease-causing mutations in other genes (*e.g. PTPN11*, n = 213; *SOS1*, n = 56; *BRAF*, n = 49, *RAF1*, n = 23). Overall, these findings indicate that *MRAS* mutations represent a rare event in NS.

Structural and biochemical characterization of the NS-causing *MRAS* mutations

Similar to the other members of the RAS superfamily of GTPases, MRAS cycles between a GTP-bound (active) and a GDP-bound (inactive) form. The transition between the two states is tightly regulated by proteins promoting GDP release (guanine nucleotide exchange factors, GEFs) and those stimulating the basally low GTPase activity (GTPase-activating proteins, GAPs). In their GTP-bound, active state, MRAS interacts with effector proteins *via* its effector binding regions (switch I and switch II). Of note, MRAS possesses a different structure of the switch I region (residues 33 to 49) as compared to other human paralogs, which has been proposed to be based on an impaired intramolecular interaction of Thr^{45} and the γ-phosphate of GTP (23,24). Though this uniqueness, the functions of Gly^{23} and Thr^{68} in MRAS are comparable to those of the corresponding residues of other RAS paralogs, as they are part of the highly conserved guanine nucleotide binding motifs 1 and 3, which are also known as the phosphate-binding loop (Gly^{20} to Ser^{27}) and the switch II region (Asp^{67} to Arg^{83}), respectively (Fig. 2A). These amino acid residues stabilize the nucleotide bound state by contacting Asp^{67} with Ser^{27} and a water molecule coordinating the magnesium ion in the MRAS active site (Fig. 2B) (22,25). Notably, the P-loop region is critical for the GTP binding and hydrolysis and thus for the function of GAPs, which stimulate GTP hydrolysis by stabilizing the transition state of this reaction. Substitution of the glycine residue by arginine or valine causes a steric clash, resulting in an impaired or defective response of the GTPase to GAPs (26). A similar consideration applies for Thr^{68}, which is adjacent to the catalytic Gln^{71}, and is located in the interswitch region of MRAS stabilizing the active site. Based on these considerations, the p.Gly23Val/Arg and p.Thr68Ile changes are predicted to affect proper GDP/GTP exchange and GTP hydrolysis, and thus cause a gain of function effect. Based on the tight interaction of Thr^{68} with the switch II, however, a perturbation of proper binding with effector proteins as the result of the substitution of this residue by isoleucine cannot be ruled out.

To evaluate the impact of the mutations on MRAS functional behavior, HEK 293 T cells were transiently transfected to express wild-type MRAS or each of three generated mutants ($MRAS^{G23R}$, $MRAS^{G23V}$ and $MRAS^{T68I}$) and the active state and subcellular localization of the GTPases were assessed. Pull-down assays directed to measure the GTP-bound levels of the four Myc-tagged proteins revealed a higher level of GTP-bound $MRAS^{G23R}$, $MRAS^{G23V}$ and $MRAS^{T68I}$ compared to the wild-type protein in both serum-free condition and following EGF stimulation (Fig. 3A). This finding indicates hyperactivation of the three mutants, which is likely to be the result of defective nucleotide binding and/or impaired GTPase activity, as predicted by the structural analysis.

Localization of RAS proteins is finely modulated, and controls the specific activation of different signaling platforms, which mediate both the extent and dynamics of signal flow and the differential activation of effectors. Based on these considerations, we assessed the subcellular localization of wild-type and mutant MRAS proteins. To this goal, immunofluorescence microscopy analysis was performed in COS-1 cells transiently expressing the Myc-tagged MRAS constructs. The wild-type MRAS protein was widely distributed in endomembranes in cells under serum-starved condition, but massively translocated to the plasma membrane following stimulation, as shown by the extensive colocalization with cortical actin (Fig. 3B). In contrast, $MRAS^{G23R}$, $MRAS^{G23V}$ and $MRAS^{T68I}$ appeared to be specifically targeted to the cell membrane both in serum-starved and EGF-stimulated cells. Of note, it has been shown that the dynamic redistribution in intracellular membranes of the RAS proteins includes their reallocation in structurally distinct microdomains of the plasma membrane. Among these, lipid rafts are cholesterol/sphingolipid-rich domains documented to serve as reservoirs for inactive signal transducers or sorting platforms for signal transduction mediating both compartmentalization and fine tuning of signaling events (27–29). By using

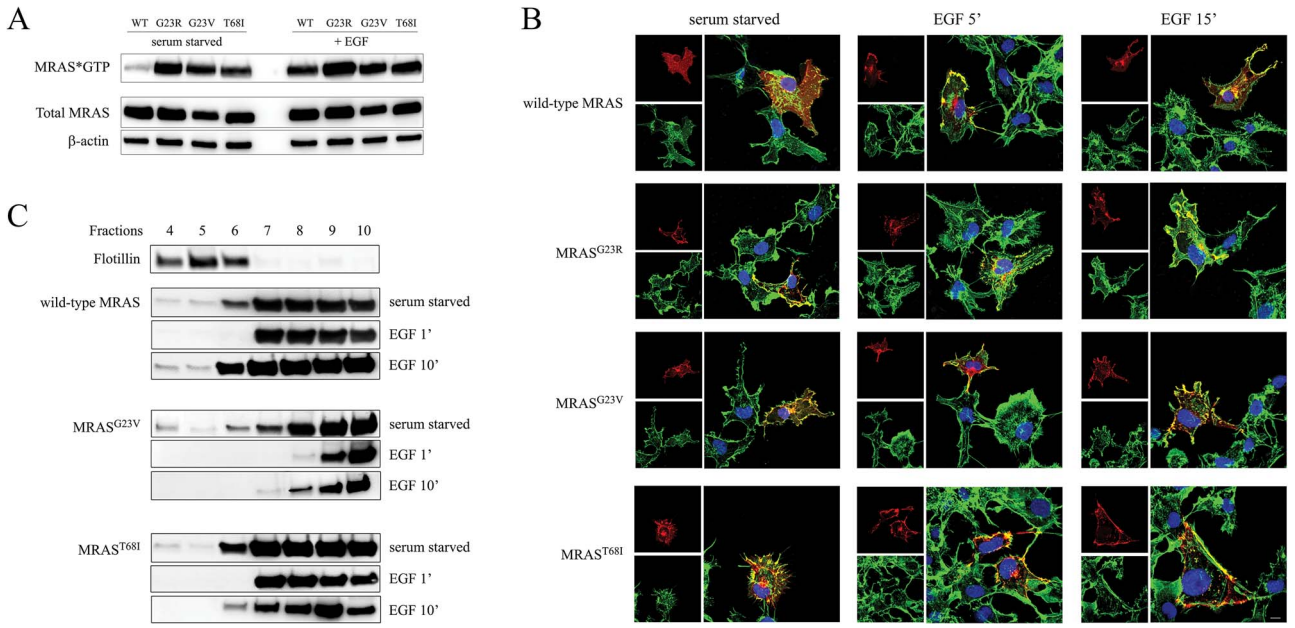

Figure 3. Biochemical and functional characterization of the MRAS mutants. A, Determination of active GTP-bound MRAS levels in HEK 293 T cells transiently expressing wild-type or mutant Myc-tagged MRAS proteins. Pull-down assays were performed using glutathione S-transferase fused to the RAS binding domain of the RAF1 kinase (GST-RAF1-RBD) in serum starved condition or after EGF (30 ng/ml) stimulation for 5 min. An anti-Myc antibody was used for MRAS detection and the β-actin was utilized as loading control. **B**, Subcellular localization of transiently expressed Myc-tagged wild-type or mutated MRAS proteins in COS-1 cells during starvation or following EGF stimulation revealed by confocal microscopy analysis. Cells were stained with anti-Myc antibody and Alexa Fluor 594 goat anti-mouse secondary antibody (red). The F-actin dye Alexa Fluor 488 phalloidin was used to stain the cortical actin associated with the plasma membrane (green). Merged images with nuclei (blue) are displayed on the right panels. Colocalization of MRAS with F-actin is shown in yellow. Note the extensive colocalization of the MRAS mutants with cortical actin even in the absence of EGF stimulation. Scale bar, 10 µm. **C**, Membrane microdomain partitioning of Myc-tagged wild-type and mutant MRAS proteins transiently expressed in HEK 293 T cells, serum starved and then stimulated with EGF (30 ng/ml) or left untreated. Wild-type and mutant MRAS proteins localize in both insoluble fractions (fractions 4 to 6, containing lipid rafts) and soluble fractions (fractions 7 to 10, including other membrane domains and cytosol) basally. Note that the relocalization of MRAS mutants in the lipid rafts after 10 min of stimulation with EGF is retarded compared to that of wild-type protein. The detergent-insoluble lipid rafts were separated by sucrose gradient ultracentrifugation, and fractions were analyzed by western blotting using flotillin as lipid raft marker.

cell fractionation experiments, localization of MRAS in lipid rafts was found to be dynamic since it was distributed in insoluble fractions containing lipid rafts (fractions 4–6) as well as in soluble fractions (fractions 7–10), the latter including proteins located in other membrane domains or in the cytosol, under serum starved condition (Fig. 3C). The GTPase translocated to non-raft domains of the plasma membrane following 1 minute of EGF stimulation, but redistributed from non-raft to raft domains after 10 minutes of stimulation, strongly suggesting that MRAS exerts its function in non-raft plasma membrane subdomains, similarly to what documented for HRAS (30,31). We assessed the dynamic distribution of the MRAS^{G23V} and MRAS^{T68I} mutants in different plasma membrane domains. As we previously documented for other RAS mutants (32), differently from the wild-type protein, a prolonged localization of both MRAS^{G23V} and MRAS^{T68I} in non-rafts fractions was appreciated (Fig. 3C). This finding and the prevalent GTP-bound state of both MRAS^{G23V} and MRAS^{T68I} proteins supports the idea that, similarly to what has been reported for HRAS, hyperactive MRAS mutants are preferentially associated with non-raft domains of the plasma membrane.

NS-causing *MRAS* mutations promote enhanced MAPK and PI3K-AKT signaling and increased binding to SHOC2 and PPP1CB

To evaluate the consequences of constitutive activation of the mutants on intracellular signaling, the extent of ERK and AKT phosphorylation was assessed. Transient overexpression of the MRAS^{G23V} and MRAS^{T68I} mutants in HEK 293 T cells was found to promote only a slightly increased, transient EGF-dependent ERK phosphorylation after 5 minutes of stimulation. By contrast, a more evident increased level of AKT phosphorylation was observed basally in cells expressing each of the two mutants (Fig. 4A). Increased levels of phosphorylated AKT were further boosted by EGF stimulation. Remarkably, the same assays performed in transiently transfected Neuro2A cells provided evidence for a significantly enhanced stimulus-dependent ERK phosphorylation promoted by the three MRAS mutants and confirmed the constitutive increased level of AKT phosphorylation even though to a lesser extent (Fig. 4B). These data document that the three MRAS mutants behave as hypermorph proteins promoting the activation of the RAF-MEK-ERK and PI3K-AKT pathways, with a modulatory effect depending on the cellular context in both cascades, at least in our experimental conditions.

MRAS positively modulates MAPK signaling by promoting SHOC2-mediated translocation of the catalytic protein phosphatase 1 (PP1C) subunit to the plasma membrane, which is a required step for a stable interaction of RAF1 with RAS proteins and subsequent activation of the kinase (33). Based on these considerations, we evaluated the binding properties of the three MRAS mutants to both SHOC2 and PPP1CB, the latter being one of the three catalytic PP1 subunits. Co-immunoprecipitation assays were performed using cell lysates collected from Neuro2A cells transiently co-expressing each of the four Myc-tagged MRAS proteins with V5-tagged SHOC2 (Fig. 4C, left panel). As shown, the three mutants showed an increased binding to

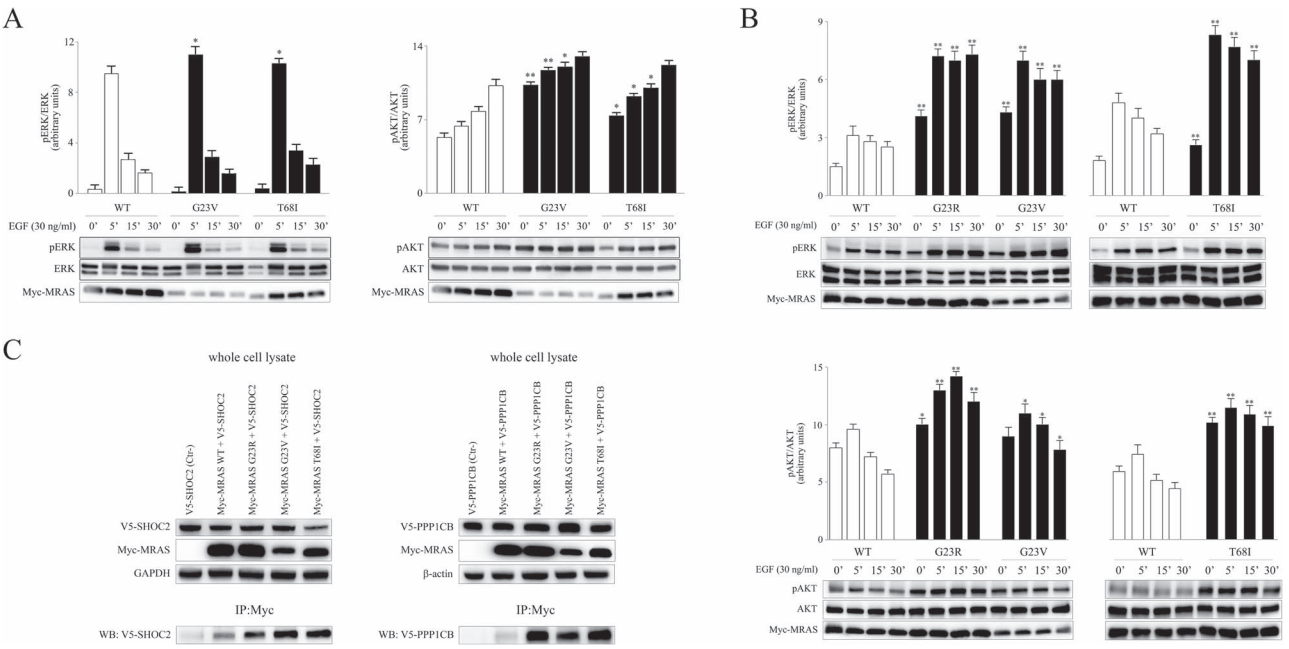

Figure 4. Disease-causing *MRAS* mutations promote enhanced activation of the MAPK and PI3K-AKT pathways. A, Transient overexpression of MRAS mutants in HEK 293 T cells promotes enhanced AKT phosphorylation basally and after EGF stimulation, and a weak increased stimulus-dependent phosphorylation of ERK, as assessed by time-course experiments. Representative blots (below) and mean ± SD densitometry values (above) of three independent experiments are shown. HEK 293 T cells were transiently transfected with the Myc-tagged MRAS constructs, serum starved and treated with 30 ng/ml EGF for 5, 15 or 30 min or left unstimulated. Equal amounts of cell lysates were resolved on 10% polyacrylamide gel. Asterisks indicate significant differences compared with wild-type MRAS at the corresponding time upon EGF stimulation (*$P < 0.05$, **$P < 0.01$; Student's t-test). **B**, Transient overexpression of MRAS mutants in Neuro2A cells promotes enhanced stimulus-dependent ERK phosphorylation (above) and increases the level of AKT phosphorylation (below) basally and after growth factor stimulation, as assessed by time-course experiments. Experiments were performed as reported above. **C**, NS-causing MRAS mutants show enhanced/more stable binding to SHOC2 and PPP1CB. Co-immunoprecipitation assays were performed using cell lysates collected from Neuro2A cells transiently co-expressing each of the four Myc-tagged MRAS proteins with V5-tagged SHOC2 (left panel) or V5-tagged PPP1CB (right panel).

SHOC2 when compared to the wild-type protein. Similarly, co-immunoprecipitation analyses using lysates collected from cells transfected to co-express the Myc-tagged MRAS proteins with V5-tagged PPP1CB documented an augmented binding of the three mutants to the catalytic subunit of PP1 compared to wild-type MRAS (Fig. 4C, right panel). These data indicate that the three NS-causing *MRAS* mutations are activating and enhance signaling through the MAPK cascade by promoting an increased and/or more stable binding of MRAS to both SHOC2 and PP1C, which is in line with recently published data (34).

Discussion

Here, we report on two patients in whom the clinical diagnosis of NS was found to be causally associated with *de novo* activating mutations of *MRAS*, and provide biochemical and functional data documenting the activating effect of these mutations on MAPK and PI3K-AKT signaling. Our findings strengthen a recent report proposing the involvement of upregulated MRAS function in NS, emphasize the association between *MRAS* mutations and HCM, and support the view that multiple signaling pathways triggered by MRAS functional upregulation are likely implicated in disease pathogenesis.

MRAS mutations had previously been reported to underlie NS in two unrelated subjects (22). One patient was a 15-year-old girl with clinical features fitting NS and having cardiac hypertrophy. Trio-based whole exome sequencing revealed a *de novo* missense mutation (c.68G > T, p.Gly23Val). The second subject was heterozygous for a different *de novo* *MRAS* variant (c.203C > T, p.Thr68Ile), identified by the same team through targeted mutational analysis in 109 unrelated patients with a suspected RASopathy and concomitant cardiac hypertrophy, who had previously been tested negative for mutations in previously identified genes implicated in NS. Notably, the latter variant is identical to the one identified as a *de novo* event in patient 1 of the present report, while the other missense change reported by Higgins et al. (22) affects the same codon as in our patient 2. These findings indicate that a narrow spectrum of missense mutations of *MRAS* cause NS. In the present study, patient 1 was the only case identified with a *MRAS* mutation among 288 individuals with a clinical diagnosis of a RASopathy who had previously been tested negative for all known RASopathy-associated genes, and no *MRAS* mutation was identified in an unselected cohort of 1840 subjects with a clinical diagnosis of RASopathy or with features suggestive of these disorders. We therefore assume that the frequency of *MRAS*-related NS is relatively rare.

The RAS superfamily of GTP/GDP-binding proteins includes a number of membrane-associated GTPases that control several cellular processes in response to a variety of extracellular stimuli, by cycling between an active, GTP-bound state and an inactive, GDP-bound state (20,21,35). Within this large group, a relatively small subfamily of structurally and functionally related proteins (*i.e.* HRAS, NRAS, and two KRAS isoforms) play a major role in controlling key cellular processes (*e.g.* proliferation, differentiation, survival and metabolism) as well as early and late developmental programs. Their importance in these processes is exemplified by the role of somatic mutations in these genes as driver events in oncogenesis, and the involvement of these genes in RASopathies when their mutations have germline origin (1–3,36; COSMIC database,

https://cancer.sanger.ac.uk/cosmic). Germline mutations in *NRAS* account for a small proportion of NS, while those affecting *HRAS* and *KRAS* underlie CS and a fraction of CFCS and NS, respectively (37–41). A closely related subfamily of GTPases includes RRAS, RRAS2 and MRAS. Similarly to the classical p21 RAS proteins, these GTPases control multiple cellular and developmental processes, and contribute to cancer when mutated (COSMIC database). Remarkably, recent studies have also established that activating mutations in these proteins underlie a small fraction of NS or related phenotypes when inherited from the germline (22,42–44). Likewise the other RAS members, MRAS is a membrane-associated protein. It shares about 50% sequence identity with the four classical p21 RAS proteins, and a higher level of conservation within the regions that mediate GTP/GDP binding and interactions with positive and negative regulators, and several effector proteins (20,21,35,45). MRAS is expressed in multiple tissues and cell types (Human Protein Atlas, https://www.proteinatlas.org/), and participates in a wide variety of signaling pathways with functions in various biological processes including bone and neural tissue formation (45–49). While MRAS has been shown to be a relatively weak activator of the RAF-MEK-ERK cascade when compared to HRAS, it has been reported to more efficiently enhance PI3K-AKT signaling (50). Higgins and colleagues were able to show that p.Gly23Val results in a protein that is more abundant in its active GTP-bound form and that weakly enhances MAPK signaling in response to growth factors (22). Biochemical/functional validation assays were not performed for the p.Thr68Ile variant. In a more recent study, the two MRAS mutants, p.Gly23Val and p.Thr68Ile, have been shown to confer MAPK pathway upregulation (34). Those observations are consistent with our findings indicating an activating role of all the three NS-causing *MRAS* mutations in promoting a GTP-bound, active state of the GTPase, its steady targeting to the plasma membrane, and a variable upregulation of the MAPK cascade, which however appears to be dependent on the cellular context. Of note, we observed that all mutants are also able to substantially upregulate the PI3K-AKT cascade, at both the basal level and upon EGF stimulation, which is in line with the known modulatory role of MRAS on this signal cascade (50).

In the context of the RAF-MEK-ERK signaling cascade, MRAS has specific functions that appear to be unique among the RAS family: active GTP-bound MRAS together with SHOC2 form a ternary complex with PP1C that has a key role in promoting SHOC2-mediated PP1C translocation to the plasma membrane, which is required for dephosphorylating a regulatory serine residue of RAF1 inhibiting stable interaction of the kinase with RAS proteins (33,34). Remarkably, missense mutations in *SHOC2* and *PPP1CB* cause Mazzanti syndrome (51,52), a RASopathy clinically related to NS, by promoting a more stable and/or prolonged formation of the complex, which in turn promotes an enhanced and sustained activation of the MAPK cascade (34, 51; our present and unpublished observations). We originally reported that the recurrent missense change in SHOC2 (p.Ser2Gly) underlying Mazzanti syndrome promotes *N*-myristoylation and constitutive plasma membrane targeting of the mutant protein, and enhanced ERK activation in a cell type-specific fashion (51). Recent studies have shown that myristylated SHOC2 has enhanced/stable binding to both MRAS and PPP1CB (34), suggesting a more efficient plasma membrane targeting of the ternary complex. Young and colleagues also demonstrated a similar behavior for disease-causing MRAS and PPP1CB mutants, which were further confirmed by the present observations, supporting a model in which the perturbing role of *SHOC2*, *PPP1CB* and *MRAS* mutations on MAPK signaling is exerted by enhancing the MRAS-SHOC2-PPP1CB complex formation at the plasma membrane, with consequent more efficient/prolonged RAF1 dephosphorylation at Ser^{259} (34). Notably, the constitutive targeting of all MRAS mutants and their abnormal cycling between lipid rafts and non-raft membrane microdomains here documented reinforce the concept of the required targeting of this protein to the plasma membrane for the specific function of the MRAS-SHOC2-PPP1CB complex, and that formation and function of this ternary complex is attained in non-raft microdomains of the plasma membrane.

Missense changes p.Gly13Arg and p.Thr58Ile in KRAS, NRAS, and HRAS, which are corresponding to p.Gly23Arg and p.Thr68Ile in MRAS, have been reported in tumors, mosaic RASopathies and RASopathies (*i.e.* NS and Costello syndrome) (Supplementary Material, Table S1), respectively, and have activating effects (39,53–55). HRAS substitutions at codon 13 (*e.g.* p.Gly13Cys, p.Gly13Ser, and Gly13Val) have been shown to confer impaired GAP-stimulated GTPase acivity (56). Similarly, mutant RAS proteins with the p.Thr58Ile substitution have been shown to upregulate the function of the protein, even though with a milder extent compared with the Gly^{12} and Gly^{13} changes (25,39,54). As in the case of $KRAS^{T58I}$ (25), substitution at Thr^{68} to Ile in MRAS most likely leads to increased GDP/GTP exchange and thus to its accumulation in the active state of the GTPase. Being integral parts of the nucleotide binding motifs of MRAS, Gly^{23} is responsible for binding to the phosphate groups of GTP/GDP, while Thr^{68} contacts Ser^{27} and Asp^{67} from the P-loop and switch II region of MRAS and is involved in magnesium ion coordination. Substitution of Gly^{23} and Thr^{68} thus is predicted to impair GTP hydrolysis and GTP/GDP binding, respectively, thereby promoting an overall stabilized GTP-bound state of the protein and enhanced downstream signaling, which was confirmed experimentally.

Analysis of clinical characteristics of the two previously published cases with *MRAS* mutations and the ones reported here shows that generally the individuals affected by these mutations appear to have all the characteristic signs and symptoms of NS, making it impossible at the current stage to distinguish *MRAS* mutation-related NS from NS of other genetic etiologies. Of note, the presence of cardiac hypertrophy in all four patients reported to date suggests that *MRAS* belongs to the NS genes with particular association to HCM (similar to *RAF1* and *RIT1*). This was already suggested by Higgins et al. (22) and it is further corroborated by the two additional observations we present here. The course of HCM was variable in the four patients with *MRAS* mutation-related NS known so far. One patient reported in the original paper required myectomy for biventricular outflow tract obstruction at age 8 years, while little information is available from the second case. The present patient 2 displayed progressive HCM leading to early lethality. This patient had the most severe outcome, which may be related to more severe activating effects of this particular mutation.

Based on the specific association between heterozygous mutations in genes encoding other partners of the complex, SHOC2 and PPP1CB, and Mazzanti syndrome, activating mutations in *MRAS* gene might also be anticipated to lead to phenotypic features characteristic of this RASopathy (*e.g.* loose anagen hair, characteristic facies, high frequency of growth hormone deficiency). However, typical phenotypic features of Mazzanti syndrome have not been documented in the previously reported cases and were not obvious in the present patients either. While the number of reported individuals with *MRAS* mutations are insufficient to make a final conclusion about a

possible relation of *MRAS* mutations with Mazzanti syndrome, the available clinical data support the idea that *MRAS* mutations are specifically linked to NS, which is likely to be associated with the more articulated impact of dysregulated *MRAS* function on intracellular signaling (e.g. enhanced PI3K-AKT signaling).

We documented that depending upon the cellular context, NS-causing MRAS mutants differentially impact MAPK and PI3K-AKT signaling cascades. This finding has relevant clinical implications, which are linked to the current effort to generate pharmacological targeted therapeutic approaches to treat the evolutive complications of RASopathies, including HCM. Indeed, accumulated evidence indicates that both the MAPK and PI3K-AKT-mTOR pathways contribute to HCM in RASopathies. Enhanced MAPK signaling has been demonstrated to contribute to HCM in the case of activating NS-causing mutations affecting *PTPN11*, *SOS1* and *RAF1* in multiple experimental models (57–59). These findings suggest that blockade of MAPK signaling by inhibitors targeting signal transducers participating in this cassette (*e.g.* the MEK inhibitor, PD0325901) could be efficacious in post-natal treatments directed to block the emergence of HCM or disease progression, depending upon when therapy is initiated. On the other hand, a specific class of mutations of *PTPN11* affecting the catalytic activity of the phosphatase and causing LEOPARD syndrome has been demonstrated to promote enhanced signaling through the PI3K-AKT-mTOR cascade (60). In this case, treatment with rapamycin, a drug specifically targeting MTOR, was found to prevent the emergence of HCM or reverse it depending on the age at which the drug was started in a mouse model of disease (61–63). These observations indicate that multiple pathways underlie HCM in RASopathies, and that distinct therapeutic approaches tailored for the specific molecular perturbation are required. For these reasons, understanding of the mechanism of disease is a required step for the identification of appropriate small molecules directed to treat HCM in RASopathies, including the form of NS caused by *MRAS* mutations.

In conclusion, the demonstration of *de novo* activating *MRAS* mutations in two patients with NS reinforces the evidence causally linking variants in *MRAS* to NS and confirms codons 23 and 68 as hot spots for NS-associated mutations in this gene. Importantly, our findings further strengthen the specific association of *MRAS* mutations with HCM and point to both the MAPK and PI3K-AKT-mTOR pathways as contributing to disease pathogenesis. Further studies are required to dissect the specific contribution of individual signaling cascades in HCM, a major evolutive complication of *MRAS*-associated NS, to the design of targeted therapeutic approaches.

Materials and Methods

Mutation screening

Diagnostic genetic analysis was performed after obtaining parental consent according to national regulations. Genomic DNA derived from venous blood samples was analyzed by sequencing of a custom multi-gene panel covering the previously published RASopathy genes (*PTPN11*, *SOS1*, *SOS2*, *RAF1*, *RIT1*, *KRAS*, *NRAS*, *RRAS*, *HRAS*, *MRAS*, *SHOC2*, *LZTR1*, *CBL*, *CDC42*, *A2ML1*, *BRAF*, *MAP 2 K1*, *MAP 2 K2*, *NF1*, *SPRED1*, *PPP1CB*, and *RASA2*). Coverage was >50x for the entire coding region of the aforementioned genes. Enrichment of exonic and flanking intronic regions of these genes was achieved using a Nextera Rapid Capture Custom Enrichment Kit (Illumina, San Diego, CA) (patient 1) and a custom SureSelect XT Target Enrichment kit (Agilent Technologies Inc., Santa Clara, CA) (patient 2). Libraries were analyzed by parallel sequencing on a MiSeq (patient 1)/NextSeq 500 (patient 2) Sequencing System (Illumina). Obtained reads were aligned and compared to the reference sequences (hg37) using the CLC Genomics Workbench (Quiagen, Venlo, The Netherlands). Filtering of variants was based on occurrence in public databases (MAF < 0.5% in ExAC and gnomAD) and predicted functional impact (PolyPhen-2, SIFT, MutationTaster, PROVEAN, and CADD). Identified variants of presumed pathogenic relevance were validated on the original DNA sample as well as parental DNA samples using conventional Sanger sequencing on an automated capillary sequencer (3500xL Genetic Analyzer, Applied Biosystems, Foster City, CA).

Structural analysis

The crystal structure of active, GppNHp-bound MRAS (PDB: 1X1S) was used to assess the impact of the identified substitutions affecting residues Gly^{23} and Thr^{68} (Gly^{13} and Thr^{58} in HRAS). To elucidate the consequence of the NS-causing mutations on GTP hydrolysis function, the structure of HRAS in complex with the catalytic domain of p120 RASGAP (PDB: 1WQ1) was analyzed, using Pymol molecular viewer (64).

Antibodies

The following antibodies were used: mouse monoclonal anti-Myc, rabbit polyclonal anti-p44/42 MAPK, mouse monoclonal anti-phospho-p44/42 MAPK (Thr^{202}/Tyr^{204}), rabbit monoclonal anti-AKT, rabbit monoclonal anti-phospho-AKT (Ser473) (Cell Signaling Technology, Danvers, MA); mouse monoclonal anti-Flotillin (BD Transduction Laboratories, Franklin Lakes, NJ); mouse monoclonal anti-V5 (Invitrogen, Carlsbad, CA); mouse monoclonal anti-GAPDH (Santa Cruz, Dallas, CA); mouse monoclonal anti-β-actin, horseradish peroxidase-conjugated anti-rabbit or anti-mouse (Sigma-Aldrich); anti-mouse conjugated to Alexa Fluor 594 (Molecular Probes, Eugene, OR).

Constructs

The entire coding sequence of wild-type (WT) *MRAS* was cloned into the pcDNA3.1/Myc A eukaryotic expression vector (Addgene, Cambridge, MA). Mutant MRAS constructs carrying the p.Gly23Val, p.Gly23Arg and p.Thr68Ile amino acid substitutions were generated by PCR-based site-directed mutagenesis using the QuikChange II Site-Directed Mutagenesis Kit (Stratagene, La Jolla, CA). The identity of each construct was verified by bidirectional Sanger sequencing.

Cell culture, transfection, and EGF stimulation

COS-1, Neuro2A and HEK 293 T cells (American Type Culture Collection, Manassas, VA) were cultured in DMEM supplemented with 10% heat-inactivated FBS, 2 mM glutamine, 100 units/ml of penicillin and 100 µg/ml of streptomycin (Euroclone, Wetherby, UK), and maintained at 37°C in a humidified atmosphere containing 5% CO2. Subconfluent cells were transfected using the Fugene6 transfection reagent (Roche Diagnostics, Mannheim, Germany), according to the manufacturer's instructions. Serum-free DMEM and EGF (30 ng/ml) (Invitrogen, Carlsbad, CA) were utilized to starve and stimulate cells, respectively.

Immunoblotting

Assays were preformed as previously reported (8,65). Briefly, cells were lysed in radio-immunoprecipitation assay (RIPA) buffer, pH 8.0, containing 20 mM NaF, 1 mM Na_3VO_4 and protease inhibitors. Lysates were kept on ice for 30 min and then centrifuged at 16000 *g* for 20 min at 4°C. Supernatants were collected and their protein concentration was determined by bicinchoninic acid (BCA) assay (66), using bovine serum albumin (BSA) as a standard. Load samples containing equal amount of total proteins were resolved by 10% sodium dodecyl sulphate (SDS)-polyacrylamide gel. After electrophoresis, proteins were transferred to nitrocellulose membrane using the Trans-Blot Turbo transfer system (Bio-Rad Laboratories, Hercules, CA). Blots were blocked with 5% non-fat milk powder in PBS containing 0.1% Tween-20 for 1 h and incubated with specific antibodies for 1 h. Primary and secondary antibodies were diluted in blocking solution. Immunoreactive proteins were detected by an enhanced chemiluminescence (ECL) detection kit (Pierce Biotechnology, Rockford, IL). Densitometric analysis of protein bands was performed using Alpha View SA image software (Protein Simple, Santa Clara, CA).

Confocal laser scanning microscopy

COS-1 cells (3×10^4) were seeded on glass coverslips, transfected with the various Myc-tagged constructs for 24 h, serum starved for 16 h and stimulated with EGF for 5 or 15 min. Cells were fixed with 4% paraformaldehyde for 30 min at 4°C and permeabilized with 0.5% Triton X-100 for 10 min at room temperature. Cells were then incubated with mouse anti-Myc antibody for 1 h at room temperature, rinsed twice with PBS, and incubated with a secondary goat anti-mouse antibody conjugated with Alexa Fluor 594 for 1 h at room temperature. After washing with PBS, cells were stained with Alexa Fluor 488 phalloidin dye to stain the filamentous actin (F-actin). Finally, glass coverslips were mounted on microscope slides using the Vectashield antifade medium containing DAPI (Vector Laboratories, Burlingame, CA) and analyzed by an Olympus FluoView FV1000 apparatus, using excitation spectral laser lines at 405, 488 and 568 nm. Signals from different fluorescent probes were taken in sequential scanning mode. Image processing used Adobe Photoshop 7.0 (Adobe Systems Incorporated, San Jose, CA).

RAS activation assay

RAS activation assays were carried out using a RAS activation assay kit (Millipore, Temecula, CA), according to the manufacturer's instructions. In brief, HEK 293 T cells were transfected with the various constructs for 24 h, serum starved for 16 h, stimulated with EGF for 5 min or left untreated, washed in ice-cold PBS and collected in Magnesium-containing Lysis Buffer (MLB). Cell lysates were further subjected to pull-down, using glutathione S-transferase fused to the RAS binding domain of the RAF1 kinase (GST-RAF1-RBD). Pulled down samples and whole cell lysates for immunoblotting analyses were mixed with sample buffer and denatured at 95°C for 5 min.

Isolation of lipid raft-enriched membrane fractions

Lipid raft-enriched membrane fractions were isolated as previously described (32,65,67). Briefly, HEK 293 T cells were transfected with different constructs for 24 h, starved 4 h, stimulated with EGF at the specified time or left untreated, rinsed twice with cold PBS, and harvested in MES-buffered saline [(MBS) 25 mM 2-(N-morpholino) ethanesulfonic acid, pH 6.5, 150 mM NaCl] containing 1% Triton X-100, 1 mM Na_3VO_4 and protease inhibitors. Each cell lysate was Dounce homogenized, adjusted to 40% sucrose and placed at the bottom of an ultracentrifuge tube. A 5–30% linear sucrose gradient was then placed above the homogenate and the mixture was centrifuged at 45000 rpm for 18 h at 4°C in a SW60Ti rotor (Beckman Instruments, Palo Alto, CA). Twelve fractions were harvested from top of gradient and stored at—20°C until analysis.

Co-immunoprecipitation assays

For co-immunoprecipitation (co-IP) analyses, Neuro2A cells were co-transfected with wild-type *SHOC2* (pcDNA6-V5-SHOC2) or *PPP1CB* (pcDNA6-V5-PPP1CB), and each of the various *MRAS* constructs for 24 h, serum starved for 16 h, stimulated with EGF for 5 min, and then lysed in IP buffer containing 25 mM Tris-HCl, pH 7.4, 1% Triton X-100, 2 mM EDTA, pH 8.0, 150 mM NaCl and protease inhibitors. Samples were centrifuged at 10000 *g* for 20 min at 4°C, supernatants were collected, and equal amounts of total proteins were immunoprecipitated with 2 µg of anti-Myc antibody for 2 h at 4°C, followed by a 2 h incubation with 20 µL protein G-sepharose beads (GE Healthcare, Freiburg, Germany) at 4°C. The beads were recovered by centrifugation and washed six times with IP buffer. Finally, the immunoprecipitated proteins were eluted with sample buffer by incubating for 5 min at 95°C and stored at −20°C for western blot analyses.

Supplementary Material

Supplementary Material is available at *HMG* online.

Acknowledgements

We thank the families for participation. This work was supported by grants from the German Federal Ministry of Education and Research (GeNeRARe, to M.R.A. [01GM1519D and 01GM1902C] and M.Z. [01GM1519A]), E-Rare (NSEuroNet, to H.C., M.R.A. [01GM1602B], M.T., and M.Z. [01GM1602A]), German Research Foundation (to M.Z. [ZE 524/10-1]), AIRC (to M.T. [IG 21614]), and Italian Ministry of Health (Ricerca Corrente 2018 and 2019, to M.T.).

Conflict of Interest statement. The authors do not have any conflict of interest.

References

1. Tartaglia, M. and Gelb, B.D. (2010) Disorders of dysregulated signal traffic through the RAS-MAPK pathway: phenotypic spectrum and molecular mechanisms. *Ann. N. Y. Acad. Sci.*, **1214**, 99–121.
2. Rauen, K.A. (2013) The RASopathies. *Annu. Rev. Genomics Hum. Genet.*, **14**, 355–369.
3. Tajan, M., Paccoud, R., Branka, S., Edouard, T. and Yart, A. (2018) The RASopathy family: consequences of Germline activation of the RAS/MAPK pathway. *Endocr. Rev.*, **39**, 676–700.
4. Roberts, A.E., Allanson, J.E., Tartaglia, M. and Gelb, B.D. (2013) Noonan syndrome. *Lancet*, **381**, 333–342.
5. Tartaglia, M., Gelb, B.D. and Zenker, M. (2011) Noonan syndrome and clinically related disorders. *Best Pract. Res. Clin. Endocrinol. Metab.*, **25**, 161–179.

6. Grant, A.R., Cushman, B.J., Cave, H., Dillon, M.W., Gelb, B.D., Gripp, K.W., Lee, J.A., Mason-Suares, H., Rauen, K.A., Tartaglia, M. *et al.* (2018) Assessing the gene-disease association of 19 genes with the RASopathies using the ClinGen gene curation framework. *Hum. Mutat.*, **39**, 1485–1493.
7. Johnston, J.J., van der Smagt, J.J., Rosenfeld, J.A., Pagnamenta, A.T., Alswaid, A., Baker, E.H., Blair, E., Borck, G., Brinkmann, J., Craigen, W. *et al.* (2018) Autosomal recessive Noonan syndrome associated with biallelic LZTR1 variants. *Genet. Med.*, **20**, 1175–1185.
8. Motta, M., Fidan, M., Bellacchio, E., Pantaleoni, F., Schneider-Heieck, K., Coppola, S., Borck, G., Salviati, L., Zenker, M., Cirstea I.C. *et al.* (2018) Dominant Noonan syndrome-causing LZTR1 mutations specifically affect the kelch domain substrate-recognition surface and enhance RAS-MAPK signaling. *Hum. Mol. Genet.*, **28**, 1007–1022.
9. Pagnamenta, A.T., Kaisaki, P.J., Bennett, F., Burkitt-Wright, E., Martin, H.C., Ferla, M.P., Taylor, J.M., Gompertz, L., Lahiri, N., Tatton-Brown, K. *et al.* (2019) Delineation of dominant and recessive forms of LZTR1-associated Noonan syndrome. *Clin. Genet.*, **95**, 693–703.
10. Sini, P., Cannas, A., Koleske, A.J., Di Fiore, P.P. and Scita, G. (2004) Abl-dependent tyrosine phosphorylation of Sos-1 mediates growth-factor-induced Rac activation. *Nat. Cell Biol.*, **6**, 268–274.
11. Holly, S.P., Larson, M.K. and Parise, L. (2005) The unique N-terminus of R-ras is required for Rac activation and precise regulation of cell migration. *Mol. Biol. Cell*, **16**, 2458–2469.
12. Kaduwal, S., Jeong, W.J., Park, J.C., Lee, K.H., Lee, Y.M., Jeon, S.H., Lim, Y.B., Min do, S. and Choi, K.Y. (2015) Sur8/Shoc2 promotes cell motility and metastasis through activation of Ras-PI3K signaling. *Oncotarget*, **6**, 33091–33105.
13. Martinelli, S., Krumbach, O.H.F., Pantaleoni, F., Coppola, S., Amin, E., Pannone, L., Nouri, K., Farina, L., Dvorsky, R., Lepri, F. *et al.* (2018) Functional Dysregulation of CDC42 causes diverse developmental phenotypes. *Am. J. Hum. Genet.*, **102**, 309–320.
14. Meyer Zum Buschenfelde, U., Brandenstein, L.I., von Elsner, L., Flato, K., Holling, T., Zenker, M., Rosenberger, G. and Kutsche, K. (2018) RIT1 controls actin dynamics via complex formation with RAC1/CDC42 and PAK1. *PLoS Genet.*, **14**, e1007370.
15. Pandit, B., Sarkozy, A., Pennacchio, L.A., Carta, C., Oishi, K., Martinelli, S., Pogna, E.A., Schackwitz, W., Ustaszewska, A., Landstrom, A. *et al.* (2007) Gain-of-function RAF1 mutations cause Noonan and LEOPARD syndromes with hypertrophic cardiomyopathy. *Nat. Genet.*, **39**, 1007–1012.
16. Razzaque, M.A., Nishizawa, T., Komoike, Y., Yagi, H., Furutani, M., Amo, R., Kamisago, M., Momma, K., Katayama, H., Nakagawa, M. *et al.* (2007) Germline gain-of-function mutations in RAF1 cause Noonan syndrome. *Nat Genet.*, **39**, 1013–1017.
17. Yaoita, M., Niihori, T., Mizuno, S., Okamoto, N., Hayashi, S., Watanabe, A., Yokozawa, M., Suzumura, H., Nakahara, A., Nakano, Y. *et al.* (2016) Spectrum of mutations and genotype-phenotype analysis in Noonan syndrome patients with RIT1 mutations. *Hum. Genet.*, **135**, 209–222.
18. Kouz, K., Lissewski, C., Spranger, S., Mitter, D., Riess, A., Lopez-Gonzalez, V., Lüttgen, S., Aydin, H., von Deimling, F., Evers, C. *et al.* (2016) Genotype and phenotype in patients with Noonan syndrome and a RIT1 mutation. *Genet. Med.*, **18**, 1226–1234.
19. Calcagni, G., Baban, A., Lepri, F.R., Marino, B., Tartaglia, M. and Digilio, M.C. (2016) Congenital heart defects in Noonan syndrome and RIT1 mutation. *Genet. Med.*, **18**, 1320.
20. Wennerberg, K., Rossman, K.L. and Der, C.J. (2005) The Ras superfamily at a glance. *J. Cell Sci.*, **118**, 843–846.
21. Nakhaei-Rad, S., Haghighi, F., Nouri, P., Rezaei Adariani, S., Lissy, J., Kazemein Jasemi, N.S., Dvorsky, R. and Ahmadian, R. (2018) Structural fingerprints, interactions, and signaling networks of RAS family proteins beyond RAS isoforms. *Crit. Rev. Biochem. Mol. Biol.*, **53**, 130–156.
22. Higgins, E.M., Bos, J.M., Mason-Suares, H., Tester, D.J., Ackerman, J.P., MacRae, C.A., Sol-Church, K., Gripp, K.W., Urrutia, R. and Ackerman, M.J. (2017) Elucidation of MRAS-mediated Noonan syndrome with cardiac hypertrophy. *JCI Insight*, **2**, e91225.
23. Ye, M., Shima, F., Muraoka, S., Liao, J., Okamoto, H., Yamamoto, M., Tamura, A., Yagi, N., Ueki, T. and Kataoka, T. (2005) Crystal structure of M-Ras reveals a GTP-bound "off" state conformation of Ras family small GTPases. *J. Biol. Chem.*, **280**, 31267–31275.
24. Matsumoto, K., Shima, F., Muraoka, S., Araki, M., Hu, L., Ijiri, Y., Hirai, R., Liao, J., Yoshioka, T., Kumasaka, T. *et al.* (2011) Critical roles of interactions among switch I-preceding residues and between switch II and its neighboring alpha-helix in conformational dynamics of the GTP-bound Ras family small GTPases. *J. Biol. Chem.*, **286**, 15403–15412.
25. Gremer, L., Merbitz-Zahradnik, T., Dvorsky, R., Cirstea, I.C., Kratz, C.P., Zenker, M., Wittinghofer, A. and Ahmadian, M.R. (2011) Germline KRAS mutations cause aberrant biochemical and physical properties leading to developmental disorders. *Hum. Mutat.*, **32**, 33–43.
26. Scheffzek, K., Ahmadian, M.R., Kabsch, W., Wiesmüller, L., Lautwein, A., Schmitz, F. and Wittinghofer, A. (1997) The Ras-RasGAP complex: structural basis for GTPase activation and its loss in oncogenic Ras mutants. *Science*, **277**, 333–338.
27. Niv, H., Gutman, O., Kloog, Y. and Henis, Y.I. (2002) Activated K-Ras and H-Ras display different interactions with saturable nonraft sites at the surface of live cells. *J. Cell Biol.*, **157**, 865–872.
28. Plowman, S.J., Muncke, C., Parton, R.G. and Hancock, J.F. (2005) H-ras, K-ras, and inner plasma membrane raft proteins operate in nanoclusters with differential dependence on the actin cytoskeleton. *Proc. Natl. Acad. Sci. U. S. A.*, **102**, 15500–15505.
29. Nicolau, D.V., Jr., Burrage, K., Parton, R.G. and Hancock, J.F. (2006) Identifying optimal lipid raft characteristics required to promote nanoscale protein-protein interactions on the plasma membrane. *Mol. Cell. Biol.*, **26**, 313–323.
30. Prior, I.A., Harding, A., Yan, J., Sluimer, J., Parton, R.G. and Hancock, J.F. (2001) GTP-dependent segregation of H-ras from lipid rafts is required for biological activity. *Nat. Cell Biol.*, **3**, 368–375.
31. Prior, I.A., Muncke, C., Parton, R.G. and Hancock, J.F. (2003) Direct visualization of Ras proteins in spatially distinct cell surface microdomains. *J. Cell Biol.*, **160**, 165–170.
32. Pantaleoni, F., Lev, D., Cirstea, I.C., Motta, M., Lepri, F.R., Bottero, L., Cecchetti, S., Linger, I., Paolacci, S., Flex, E. *et al.* (2017) Aberrant HRAS transcript processing underlies a distinctive phenotype within the RASopathy clinical spectrum. *Hum. Mutat.*, **38**, 798–804.
33. Rodriguez-Viciana, P., Oses-Prieto, J., Burlingame, A., Fried, M. and McCormick, F. (2006) A phosphatase holoenzyme comprised of Shoc2/Sur8 and the catalytic subunit of PP1

functions as an M-Ras effector to modulate Raf activity. *Mol. Cell*, **22**, 217–230.
34. Young, L.C., Hartig, N., Boned Del Rio, I., Sari, S., Ringham-Terry, B., Wainwright, J.R., Jones, G.G., McCormick, F. and Rodriguez-Viciana, P. (2018) SHOC2-MRAS-PP1 complex positively regulates RAF activity and contributes to Noonan syndrome pathogenesis. *Proc. Natl. Acad. Sci. U.S.A.*, **115**, E10576–E10585.
35. Bourne, H.R., Sanders, D.A. and McCormick, F.T. (1991) The GTPase superfamily: conserved structure and molecular mechanism. *Nature*, **349**, 117–127.
36. Bos, J.L. (1989) Ras oncogenes in human cancer: a review. *Cancer Res.*, **49**, 4682–4689.
37. Cirstea, I.C., Kutsche, K., Dvorsky, R., Gremer, L., Carta, C., Horn, D., Roberts, A.E., Lepri,F., Merbitz-Zahradnik, T., König, R. *et al.* (2010) A restricted spectrum of NRAS mutations causes Noonan syndrome. *Nat. Genet.*, **42**, 27–29.
38. Aoki, Y., Niihori, T., Kawame, H., Kurosawa, K., Ohashi, H., Tanaka, Y., Filocamo, M., Kato, K., Suzuki, Y., Kure, S. *et al.* (2005) Germline mutations in HRAS proto-oncogene cause Costello syndrome. *Nat. Genet.*, **37**, 1038–1040.
39. Schubbert, S., Zenker, M., Rowe, S.L., Boll, S., Klein, C., Bollag, G., van der Burgt, I., Musante, L., Kalscheuer, V., Whenner, L.E. *et al.* (2006) Germline KRAS mutations cause Noonan syndrome. *Nat. Genet.*, **38**, 331–336.
40. Carta, C., Pantaleoni, F., Bocchinfuso, G., Stella, L., Vasta, I., Sarkozy, A., Digilio, C., Palleschi, A., Pizzuti, A., Grammatico, P. *et al.* (2006) Germline missense mutations affecting KRAS isoform B are associated with a severe Noonan syndrome phenotype. *Am. J. Hum. Genet.*, **79**, 129–135.
41. Niihori, T., Aoki, Y., Narumi, Y., Neri, G., Cavé, H., Verloes, A., Okamoto, N., Hennekam, R.C., Gillessen-Kaesbach, G., Wieczorek, D. *et al.* (2006) Germline KRAS and BRAF mutations in cardio-facio-cutaneous syndrome. *Nat. Genet.*, **38**, 294–296.
42. Flex, E., Jaiswal, M., Pantaleoni, F., Martinelli, S., Strullu, M., Fansa, E.K., Caye, A., De Luca, A., Lepri, F., Dvorsky, R. *et al.* (2014) Activating mutations in RRAS underlie a phenotype within the RASopathy spectrum and contribute to leukaemogenesis. *Hum. Mol. Genet.*, **23**, 4315–4327.
43. Capri, Y., Flex, E., Krumbach, O.H.F., Carpentieri, G., Cecchetti, S., Lißewski, C., Rezaei Adariani, S., Schanze, D., Brinkmann, J., Piard, J. *et al.* (2019) Activating mutations of RRAS2 are a rare cause of Noonan syndrome. *Am. J. Hum. Genet.*, in press.
44. Niihori, T., Nagai, K., Fujita, A., Ohashi, H., Okamoto, N., Okada, S., Harada, A., Kihara, H., Arbogast, T., Funayama, R. *et al.* (2019) Germline activating RRAS2 mutations cause Noonan syndrome. *Am. J. Hum. Genet.*, in press.
45. Kimmelman, A., Tolkacheva, T., Lorenzi, M.V., Osada, M. and Chan, A.M. (1997) Identification and characterization of R-ras3: a novel member of the RAS gene family with a non-ubiquitous pattern of tissue distribution. *Oncogene*, **15**, 2675–2685.
46. Ehrhardt, G.R., Leslie, K.B., Lee, F., Wieler, J.S. and Schrader, J.W. (1999) M-Ras, a widely expressed 29-kD homologue of p21 Ras: expression of a constitutively active mutant results in factor-independent growth of an interleukin-3-dependent cell line. *Blood*, **94**, 2433–2444.
47. Young, L.C., Hartig, N., Munoz-Alegre, M., Oses-Prieto, J.A., Durdu, S., Bender, S., Vijayakumar, V., Vietri Rudan, M., Gewinner, C. *et al.* (2013) An MRAS, SHOC2, and SCRIB complex coordinates ERK pathway activation with polarity and tumorigenic growth. *Mol. Cell*, **52**, 679–692.
48. Watanabe-Takano, H., Takano, K., Keduka, E. and Endo, T. (2010) M-Ras is activated by bone morphogenetic protein-2 and participates in osteoblastic determination, differentiation, and transdifferentiation. *Exp. Cell Res.*, **316**, 477–490.
49. Mathieu, M.E., Faucheux, C., Saucourt, C., Soulet, F., Gauthereau, X., Fedou, S., Trouillas, M., Thézé, N., Thiébaud, P. and Boeuf, H. (2013) MRAS GTPase is a novel stemness marker that impacts mouse embryonic stem cell plasticity and Xenopus embryonic cell fate. *Development*, **140**, 3311–3322.
50. Kimmelman, A.C., Osada, M. and Chan, A.M. (2000) R-Ras3, a brain-specific Ras-related protein, activates Akt and promotes cell survival in PC12 cells. *Oncogene*, **19**, 2014–2022.
51. Cordeddu, V., Di Schiavi, E., Pennacchio, L.A., Ma'ayan, A., Sarkozy, A., Fodale, V., Cecchetti, S., Cardinale, A., Martin, J., Schackwitz, W. *et al.* (2009) Mutation of SHOC2 promotes aberrant protein N-myristoylation and causes Noonan-like syndrome with loose anagen hair. *Nat. Genet.*, **41**, 1022–1026.
52. Gripp, K.W., Aldinger, K.A., Bennett, J.T., Baker, L., Tusi, J., Powell-Hamilton, N., Stabley, D., Sol-Church, K., Timms, A.E. and Dobyns, W.B. (2016) A novel rasopathy caused by recurrent de novo missense mutations in PPP1CB closely resembles Noonan syndrome with loose anagen hair. *Am. J. Med. Genet. A*, **170**, 2237–2247.
53. Gripp, K.W., Innes, A.M., Axelrad, M.E., Gillan, T.L., Parboosingh, J.S., Davies, C., Leonard, N.J., Lapointe, M., Doyle, D., Catalano, S. *et al.* (2008) Costello syndrome associated with novel germline HRAS mutations: an attenuated phenotype? *Am. J. Med. Genet. A*, **146A**, 683–690.
54. Altmuller, F., Lissewski, C., Bertola, D., Flex, E., Stark, Z., Spranger, S., Baynam, G., Buscarilli, M., Dyack, S., Gillis, J. *et al.* (2017) Genotype and phenotype spectrum of NRAS germline variants. *Eur. J. Hum. Genet.*, **25**, 823–831.
55. Groesser, L., Herschberger, E., Ruetten, A., Ruivenkamp, C., Lopriore, E., Zutt, M., Langmann, T., Singer, S., Klingseisen, L., Schneider-Brachert, W. *et al.* (2012) Postzygotic HRAS and KRAS mutations cause nevus sebaceous and Schimmelpenning syndrome. *Nat. Genet.*, **44**, 783–787.
56. Wey, M., Lee, J., Jeong, S.S., Kim, J. and Heo, J. (2013) Kinetic mechanisms of mutation-dependent Harvey Ras activation and their relevance for the development of Costello syndrome. *Biochemistry*, **52**, 8465–8479.
57. Chen, P.C., Wakimoto, H., Conner, D., Araki, T., Yuan, T., Roberts, A., Seidman, C., Bronson, R., Neel, B., Seidman, J.G. *et al.* (2010) Activation of multiple signaling pathways causes developmental defects in mice with a Noonan syndrome–associated Sos1 mutation. *J. Clin. Invest.*, **120**, 4353–4365.
58. Wu, X., Simpson, J., Hong, J.H., Kim, K.H., Thavarajah, N.K., Backx, P.H., Neel, B.G. and Araki, T. (2011) MEK-ERK pathway modulation ameliorates disease phenotypes in a mouse model of Noonan syndrome associated with the Raf1(L613V) mutation. *J. Clin. Invest.*, **121**, 1009–1025.
59. Nakamura, T., Colbert, M., Krenz, M., Molkentin, J.D., Hahn, H.S., Dorn, G.W., 2nd and Robbins, J. (2007) Mediating ERK 1/2 signaling rescues congenital heart defects in a mouse model of Noonan syndrome. *J. Clin. Invest.*, **117**, 2123–2132.
60. Edouard, T., Combier, J.P., Nédélec, A., Bel-Vialar, S., Métrich, M., Conte-Auriol, F., Lyonnet, S., Parfait, B., Tauber, M., Salles, J.P. *et al.* (2010) Functional effects of PTPN11 (SHP2) mutations causing LEOPARD syndrome on epidermal growth factor-induced phosphoinositide 3-kinase/AKT/glycogen synthase kinase 3beta signaling. *Mol. Cell Biol.*, **30**, 2498–2507.

61. Marin, T.M., Keith, K., Davies, B., Conner, D.A., Guha, P., Kalaitzidis, D., Wu, X., Lauriol, J., Wang, B., Bauer, M. *et al.* (2011) Rapamycin reverses hypertrophic cardiomyopathy in a mouse model of LEOPARD syndrome-associated PTPN11 mutation. *J. Clin. Invest.*, **121**, 1026–1043.
62. Hahn, A., Lauriol, J., Thul, J., Behnke-Hall, K., Logeswaran, T., Schänzer, A., Böğürcü, N., Garvalov, B.K., Zenker, M., Gelb, B.D. *et al.* (2015) Rapidly progressive hypertrophic cardiomyopathy in an infant with Noonan syndrome with multiple lentigines: palliative treatment with a rapamycin analog. *Am. J. Med. Genet. A*, **167A**, 744–751.
63. Wang, J., Chandrasekhar, V., Abbadessa, G., Yu, Y., Schwartz, B. and Kontaridis, M.I. (2017) In vivo efficacy of the AKT inhibitor ARQ 092 in Noonan syndrome with multiple lentigines-associated hypertrophic cardiomyopathy. *PLoS One*, **12**, e0178905.
64. DeLano W. *The PyMOL Molecular Graphics System*, Version 1.8.2.3. DeLano Scientific LLC, San Carlos, CA. 2002.
65. Motta, M., Chillemi, G., Fodale, V., Cecchetti, S., Coppola, S., Stipo, S., Cordeddu, V., Macioce, P., Gelb, B.D. and Tartaglia, M. (2016) SHOC2 subcellular shuttling requires the KEKE motif-rich region and N-terminal leucine-rich repeat domain and impacts on ERK signalling. *Hum. Mol. Genet.*, **25**, 3824–3835.
66. Smith, P.K., Krohn, R.I., Hermanson, G.T., Mallia, A.K., Gartner, F.H., Provenzano, M.D., Fujimoto, E.K., Goeke, N.M., Olson, B.J. and Klenk, D.C. (1987) Measurement of protein using bicinchoninic acid. *Anal. Biochem.*, **150**, 76–85.
67. Sargiacomo, M., Sudol, M., Tang, Z. and Lisanti, M.P. (1993) Signal transducing molecules and glycosyl-phosphatidylinositol-linked proteins form a caveolin-rich insoluble complex in MDCK cells. *J. Cell Biol.*, **122**, 789–807.